Lawrence Berkeley National Laboratory
Recent Work

Title
Complementary use of monochromatic and white-beam X-ray micro-diffraction for the investigation of ancient materials

Permalink
https://escholarship.org/uc/item/4ft7j7c2

Journal
Journal of Applied Crystallography, 48(5)

ISSN
0021-8898

Authors
Dejoie, C
Tamura, N
Kunz, M
et al.

Publication Date
2015-10-01

DOI
10.1107/S1600576715014983

Peer reviewed

Complementary use of monochromatic and white-beam X-ray micro-diffraction for the investigation of ancient materials

Catherine Dejoie,[a] Nobumichi Tamura,[b] Martin Kunz,[b] Philippe Goudeau[c] and Philippe Sciau[d]*

[a]Laboratory of Crystallography, ETH Zurich, Vladimir-Prelog-Weg 1-5/10, Zurich 8093, Switzerland, [b]Advanced Light Source, Lawrence Berkeley National Laboratory, 1 Cyclotron Road, Berkeley, CA 94720, USA, [c]Institut Pprime, CNRS – Université de Poitiers – ENSMA, Futuroscope 86960, France, and [d]CEMES – CNRS – Université de Toulouse, 29 Rue J. Marvig, Toulouse 31055, France. *Correspondence e-mail: philippe.sciau@cemes.fr

Archaeological artefacts are often heterogeneous materials where several phases coexist in a wide grain size distribution. Most of the time, retrieving structure information at the micrometre scale is of great importance for these materials. Particularly, the organization of different phases at the micrometre scale is closely related to optical or mechanical properties, manufacturing processes, functionalities in ancient times and long-term conservation. Between classic X-ray powder diffraction with a millimetre beam and transmission electron microscopy, a gap exists and structure and phase information at the micrometre scale are missing. Using a micrometre-size synchrotron X-ray beam, a hybrid approach combining both monochromatic powder micro-diffraction and Laue single-crystal micro-diffraction was deployed to obtain information from nanometre- and micrometre-size phases, respectively. Therefore providing a way to bridge the aforementioned gap, this unique methodology was applied to three different types of ancient materials that all show a strong heterogeneity. In Roman *terra sigillata*, the specific distribution of nanocrystalline hematite is mainly responsible for the deep-red tone of the slip, while the distribution of micrometre-size quartz in ceramic bodies reflects the change of manufacturing process between pre-*sigillata* and high-quality *sigillata* periods. In the second example, we investigated the modifications occurring in Neolithic and geological flints after a heating process. By separating the diffracted signal coming from the nano- and the micrometre scale, we observed a domain size increase for nanocrystalline quartz in geological flints and a relaxation of the residual strain in larger detritic quartz. Finally, through the study of a Roman iron nail, we showed that the carburation process to strengthen the steel was mainly a surface process that formed 10–20 µm size domains of single-crystal ferrite and nanocrystalline cementite.

1. Introduction

Archaeological and historical artefacts are typically complex and heterogeneous materials showing multi-scale architectures: coexistence of crystalline and amorphous phases in glazed ceramics composed of a micrometre-sized coating supported by a body (Sciau, Relaix *et al.*, 2006; Dejoie, Sciau *et al.*, 2014), mixing of organic and inorganic components in layered paintings (Welcomme *et al.*, 2007; Dejoie, Martinetto *et al.*, 2014), or a wide crystal size distribution in Egyptian cosmetics (Walter *et al.*, 1999). In these systems, the arrangement of several components with different grain sizes is intimately linked to the intrinsic properties of the artefacts (colour, brightness, resistance to friction, waterproofing *etc.*). Revealing this arrangement and the associated morphology can provide not only information on a long-forgotten process
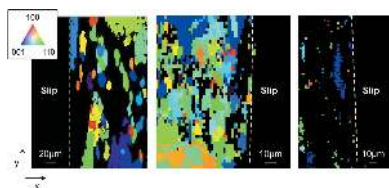
technique but also clues for the long-term conservation of such objects. Therefore, combining crystallographic data originating from different grain sizes is of fundamental importance.

Several techniques such as Raman spectroscopy and petrography can extract information at the micrometre scale, a morphological length scale which is typical and of utmost importance for most artefacts. Indeed, Raman spectroscopy and petrographic analysis can be used to rapidly characterize texture and phase composition (Ingham, 2011; Baraldi & Tinti, 2008). However, in many cases these techniques give only part of the information needed, and a complete structural description can only be achieved using X-ray diffraction (XRD) techniques. As the XRD spatial resolution is determined by the size of the incident X-ray beam, structural information in the [20–1 µm] range can only be obtained by using a micrometre to submicrometre beam size. Today, most synchrotron facilities can provide such a small beam size in a routine manner (Tamura et al., 2002; Ice et al., 2011; Bertrand et al., 2012), which has opened new possibilities for structural mapping of heterogeneous samples. In particular, X-ray powder diffraction imaging has been extensively used in several area of materials science (Goudeau et al., 2003; Xu et al., 2012; Vaxelaire et al., 2014), including the study of ancient artefacts (Dooryhée et al., 2005; De Nolf & Janssens, 2010).

A variety of structural information can be extracted from a powder diffraction pattern, from qualitative phase identification to a more quantitative analysis (volume fraction of crystalline and/or amorphous phases, crystal size and/or crystal elastic strain, etc.). For quantitative analysis, the powder diffraction method requires a large (ideally infinite) number of randomly oriented crystallites in the diffracting volume in order to collect a physically meaningful diffraction pattern. Therefore, it requires the crystallite size to be much smaller than the X-ray beam size. This condition starts to be difficult to achieve when a micrometre X-ray beam (e.g. 1×1 µm) is used. With such a beam size, only nanometre-size crystals (<100 nm) can fulfil the powder diffraction condition. For crystals of comparable or larger size than the beam size, a single-crystal diffraction technique has to be used to extract structural information. 'Classic' monochromatic single-crystal diffraction requires the rotation of a single crystal in the X-ray beam in a controlled manner. This technique is not suitable for the study of small crystallites inside a complex matrix, as often found in many archaeological artefacts.

The Laue (white-beam) single-crystal diffraction technique is an attractive alternative to the monochromatic one, because it takes full advantage of the X-ray energy spectrum delivered at a synchrotron source and requires no rotation of the crystal (Tamura et al., 2003; Ice & Pang, 2009). By using a broad energy band-pass X-ray source, a large number of reciprocal lattice points can be recorded simultaneously in a single exposure with a short recording time (<1 s) when using two-dimensional detectors. Combining Laue diffraction with an X-ray microbeam, small crystals inside a heterogeneous matrix can be probed directly and efficiently. Over the past ten years, Laue micro-diffraction has been applied successfully to

map grain orientation and crystal distortion in polycrystalline and composite materials (Tamura et al., 2003; Kunz, Chen et al., 2009). Nevertheless, only a few Laue mapping applications in relation with cultural heritage have been reported so far. Sciau, Goudeau et al. (2006) investigated the distribution of micrometre-sized quartz crystals at the surface of terra sigillata pottery using Laue micro-diffraction. Liu et al. (2007) reported the presence of $BaCuSi_2O_6$ crystals (Chinese purple) in the paintings decorating terracotta warriors from the Qin dynasty, where Laue micro-diffraction was used to investigate the orientation and the distribution of the grains in the pigment. Similar methodology has also been applied to the study of colour pigments from an ancient Egyptian coffin (747–600 BC), where the potential of Laue micro-diffraction for mineralogical phase identification was addressed (Lynch et al., 2007).

Because of the intrinsic heterogeneity of ancient materials, a mixture of both microscale and nanoscale phases is expected to coexist inside the investigated zone, giving rise to both powder-like and single-crystal-like data. Then, only the combination of monochromatic powder and Laue single-crystal micro-diffraction mapping over the same area of the samples can provide (semi-)quantitative structural information over the full spatial range. The key to implement this hybrid approach is to be able to switch efficiently between monochromatic and Laue modes locally at the same beamline, without modifying the experimental conditions by moving the sample or changing the average position of the focal point.

The objective of the present paper is to use this hybrid approach to characterize the structure at the micrometre scale of three different types of archaeological artefacts in order to get additional insights into their physical properties, in relation to their function in ancient times. To do so, a mapping of the regions of interest will be performed with a poly- and a monochromatic microbeam to get the required spatial resolution. The three selected samples show a strong heterogeneity over micrometre length scales where the role of interfaces and phase distribution, related to the material properties, needs to be understood and for which data are missing: (i) terra sigillata ceramics from the Roman period (Sciau, Relaix et al., 2006), composed of several parts (slip and body) and several phases with a grain size varying from nanometres to a few micrometres; (ii) flint tools from the Neolithic period (Ríos et al., 2001), where the main quartz phase shows a grain size heterogeneity related to its geological formation; and (iii) iron nails from the Roman period (Douin et al., 2010), composed of several phases and in which the size of the ferrite domains varies depending on their location.

2. Archaeological materials

All three archaeological samples have been previously structurally characterized either at a macroscale with a large X-ray beam where all the different phases can be seen as powder ('classic' X-ray powder diffraction) or at a nanoscale with a transmission electron microscope (imaging and diffraction) where only a very small area, which may not be representative

of the sample, can be visualized. *Terra sigillata* wares are the only example that has been investigated previously at the micrometre scale using X-ray micro-diffraction, but only for qualitative analysis and phase identification (Sciau, Goudeau *et al.*, 2006; Leon *et al.*, 2010).

2.1. Roman *terra sigillata* ceramics

Terra sigillata pottery is characteristic of the Roman period. During the first century AD, millions of wares were produced in standardized shapes at the main Gallic workshop (La Graufesenque) and distributed widely over the Roman Empire (Hermet, 1934; Schaad, 2007). The success of this tableware is mainly due to its vivid red coating (slip) (Sciau, Relaix *et al.*, 2006). The red colour of *terra sigillata* is attributed to the presence of hematite, α-Fe_2O_3, a fully oxidized iron oxide phase (Sciau, Relaix *et al.*, 2006). The red colour of hematite derives from several Fe^{3+} ligand-field transitions in the visible range and a strong ligand-to-metal charge transfer transition (O^{2-} to Fe^{3+}) in the UV range. In particular, the position of the reflectance band at ∼545 nm assigned to Fe^{3+}–Fe^{3+} pair excitations is strongly correlated to the hue. Nevertheless, the amount, the chemical composition, the size and the distribution of hematite crystals will influence the colour of the ceramics (Torrent & Barrón, 2003). By studying the microstructure of high-quality *sigillata* ceramics, the objective is to clarify the role of these different parameters (size, distribution *etc.*) in the final colour.

At the end of the first century BC, before the production of the high-quality *terra sigillata* ceramics, the workshop of La Graufesenque started to make a tableware inspired by Italian *sigillata* (often called pre-*sigillata*), by applying a fine decanted clay coating onto a coarser clay body (Mirguet *et al.*, 2009). Other Gallic workshops, like Bram, also started to produced pre-*sigillata*, without later moving to *sigillata* production (Passelac, 2004). While pre-*sigillata* was seen as a first step in the establishment of *sigillata* production, pre-*sigillata* ware is now considered as a specific type of tableware (Passelac, 2007). However, the link between these two types of tableware, in particular the preparation process of the raw clay used to obtain the coating, is still not well understood. A structural study of the phases not transformed during the firing process (*e.g.* quartz) can provide significant information on the manufacturing process. To get more insight on this and on the changes operated at the pre-*sigillata*/*sigillata* transition period at La Graufesenque, the distribution of quartz at the micrometre scale of two pre-*sigillata* samples from the Bram and La Graufesenque workshops will be compared with that from a high-quality *sigillata* of La Graufesenque.

2.2. Neolithic flints

The Chassey culture from the Vaucluse region in southern France (4200–3500 BC) developed a specialized lithic technology for the making of flint bladelets. The essential part of this process is a heating step resulting in changes of the flint's original gloss, roughness and mechanical properties (Lea, 2005). These heated flints were successfully spread over a wide geographical area from northern Italy to northern Spain (Gibaja & Terradas, 2012). Flints are sedimentary silica rocks, made of chalcedony, which consist of 50–100 nm-large quartz crystallites arranged in a fibre-like texture (Ríos *et al.*, 2001). Larger isolated detritic quartz grains (>1 μm) are also present, trapped into the chalcedony network during the geological formation (Schmidt, Lea *et al.*, 2013). A small quantity of moganite nanocrystals (<5%), a monoclinic SiO_2 polymorph (Schmidt, Lea *et al.*, 2013), may also be present. Recent studies have tried to clarify both the heating temperature (473–523 K) and the heat-induced transformations occurring in flints (Roqué *et al.*, 2011; Schmidt, Lea *et al.*, 2013; Schmidt, Slodczyk *et al.*, 2013). Upon heat treatment, silanols, Si—OH, are lost and new Si—O—Si bonds are created, according to the reaction: Si—OH HO—Si → Si—O—Si + H_2O. This leads to a 'closing of the porosity' and an improvement of the mechanical resistance at the grain boundaries, resulting in a more homogeneous distribution of mechanical strength. The production of flint bladelets by a pressure technique is thus facilitated, and the sharpness of the blades (cutting properties) is also improved.

In this study, structural changes related to the heating process in both nano-quartz and larger detritic quartz are investigated. We concentrate in particular on the evolution of the coherent domain size of the nano phase and mechanical stresses present in the larger grains of detritic quartz. Both heated and non-heated archaeological flints are investigated, and the results are compared with non-heated and heated geological flints.

2.3. Roman nail

Iron during the Roman period was produced by 'direct reduction' with charcoal (Pagès *et al.*, 2011). Because of the moderate temperature obtained in a shaft furnace (1523–1573 K), the reduction process occurred in the solid-state phase. Therefore, the resulting iron loop had to be refined by repetitive hammering and reheating to remove the slag and charcoal inclusions and to make the carbon steel more homogeneous. As such, the microstructure of archaeological iron from that period not only plays a significant role in its mechanical properties but also strongly depends on the manufacturing process. The set of nails of the present study as well as various iron artefacts have been subject to standard archaeological and archaeometry study over the past ten years (Renoux *et al.*, 2004; Renoux, 2006).

In this study, we analyse the distribution of the different phases from the top surface to the core of the nail, the correlation between these micro/nano phases (distribution, strain), and the influence of the phase distribution on material properties (hardness, elasticity). The investigated sample was previously studied by transmission electron microscopy (Douin *et al.*, 2010). We expected to get complementary and reliable information by investigating a more representative volume.

3. Experimental

3.1. Samples

The *terra sigillata* samples come from the excavations of the workshop of La Graufesenque (Aveyron, France), one of the most important centres of *terra sigillata* production during the first century AD (Déchelette, 1903; Sciau, Relaix *et al.*, 2006; Schaad, 2007). The pre-*sigillata* samples used in this study were produced by the workshops of Bram (Aude, France) (Passelac, 1992) and La Graufesenque (Mirguet *et al.*, 2009). These samples are part of a body of work performed in the framework of Y. Leon's PhD thesis (Leon, 2010). The X-ray diffraction measurements were performed on cross-section samples originally prepared for scanning electron microscopy investigations and microprobe analysis (Fig. 1*a*).

Two archaeological Chassey flint bladelets and two geological flint samples were studied. The archaeological flints come from the production site of Saint-Martin (Vaucluse, France) and were selected by V. Lea, manager of the excavation (Lea, 2005). One flake was taken from an unheated preform, while the other one was extracted from a preform after a heat treatment. The two geological flints belong to a series of samples extracted from a geological Barremo–Bedoulian nodule. These samples were heated at 673 K in an electric furnace under oxidizing atmosphere for 8 h with a heating rate of 0.2 K min^{-1}. X-ray micro-diffraction measurements were

carried out directly on the samples without any surface preparation (Fig. 1*b*).

The Roman iron nail specimen studied here belongs to a set of iron nails extracted from the excavations at Puy d'Issolud (France), where the Uxellodunum battle took place in 52 BC during the Gallic Wars (Gilliver, 2002; Renoux, 2006). The square section of the nail was slightly polished on one side and was cut perpendicularly near one of its ends. The measurements were performed on both the polished longitudinal surface and the exposed cross section (Fig. 1*c*).

3.2. Data collection and processing

Only a few beamlines over the world offer the possibility of switching between monochromatic and Laue modes locally without changing the average position of the focal point. This is the case of the 34-ID-E beamline at the Advanced Photon Source (USA), the 12.3.2 beamline at the Advanced Light Source (ALS, USA), the 4B beamline at the Pohang Light Source (Korea), Vesper at the Canadian Light Source (Canada), the forthcoming (opening in 2016) 21A beamline at the National Synchrotron Radiation Research Center (Taiwan) and, partially, the BM32 beamline at the European Synchrotron Radiation Facility (France) and the BM16 beamline at Diamond (UK). Although this methodology seems attractive to study heterogeneous materials, only a few examples in which monochromatic powder and Laue single-crystal micro-diffraction modes are combined in such a way have been reported so far (Korsunsky *et al.*, 2010). In the case of strain/stress studies, the monochromatic mode is mainly used as a complementary single-crystal technique to retrieve the true energy of each individual peak of a Laue pattern (MacDowell *et al.*, 2001; Robach *et al.*, 2011).

The monochromatic and Laue micro-diffraction experiments were conducted on Beamline 12.3.2 at the ALS (Lawrence Berkeley National Laboratory). The X-ray beam was focused down to 1 × 1 µm in polychromatic mode (5–24 keV) and 10 × 4 µm in monochromatic mode using a pair of Kirkpatrick–Baez mirrors (Tamura *et al.*, 2009; Kunz, Tamura *et al.*, 2009). The size increase for the monochromatic beam is necessary in order to get enough diffracted beam intensity and thus reasonable mapping time. A DuMont–Hart–Bartels four-bounce monochromator design allowed for fast switching between the monochromatic mode and the Laue mode, while accurately maintaining the beam position on the sample surface. Diffraction patterns were collected in reflection geometry using a two-dimensional Mar133 X-ray CCD detector. The two-dimensional detector can be moved freely to adjust the sample–detector distance and the angle 2θ (from 0 to 90°). The sample was mounted on a fast x–y stage for scanning in two directions with accuracy better than 100 nm. The inclination of the sample relative to the incident beam can be chosen, and was fixed at an angle of 30° relative to the incident beam for all the samples.

A Vortex-EM (SII Nanotech) detector was used for the collection of the X-ray fluorescence signal. Only chemical elements with emission lines higher than 3 keV (K, Z = 19) could be detected.
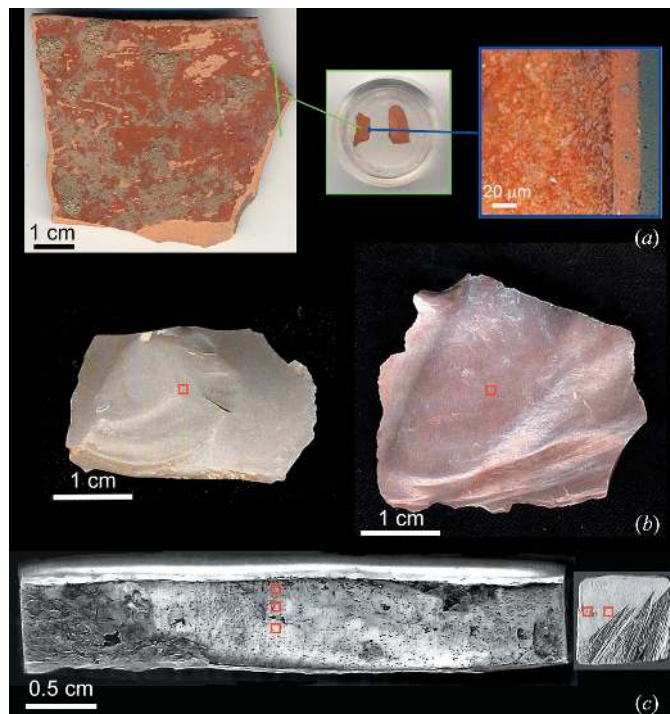

Figure 1
(*a*) Pre-*sigillata* sample from the Bram workshop. A sherd is embedded inside epoxy before observation under an optical microscope. The decorative layer (slip) and the body of the ceramic are clearly visible on the cross-section view. (*b*) Archaeological flint before (left) and after (right) the heating process. (*c*) Polished surface and cross section of the iron nail investigated. For (*b*) and (*c*), analysed zones are shown with red squares.

The experiment was conducted as follows: first, several large fluorescence maps (500 × 500 µm) were collected by raster-scanning the region of interest across the X-ray microbeam. All fluorescence maps were collected using the white-beam mode. After analysis of the chemical composition distribution in the fluorescence maps, smaller zones of interest (100 × 100 µm) were selected. Diffraction scans were then carried out in these selected areas, using monochromatic (Debye–Scherrer powder diffraction pattern) and polychromatic (single-crystal Laue diffraction pattern) modes.

Laue data were analysed using the *XMAS* software package (Tamura, 2014). The sample-to-detector distance, the normal incidence position of the detector and the tilt angle of the detector relative to the sample surface were calibrated using a Laue pattern obtained from a strain-free (001)-oriented Si wafer. Geometric and scanning parameters for all the samples are shown in Table 1. The true energy of each individual spot being unknown, only the ratio between two cell parameters (*e.g.* a/c) can be retrieved from Laue data through a unit-cell shape refinement. To do so, cell parameters are defined as vectors: **a** (ax, ay, az), **b** (bx, by, bz) and **c** (cx, cy, cz), each component being allowed to vary without symmetry constraints. The new (triclinic) cell parameters are then calculated from the refined vectors. The deviatoric part of the strain tensor (ε_{xx}, ε_{yy}, ε_{zz}, ε_{xy}, ε_{yz}, ε_{xz}) can be deduced from Laue patterns, by calculating the misfit between the indexed pattern and a reference one. The magnitude of the deviatoric strain tensor is expressed as the 'equivalent strain' $\varepsilon_{eq} = [(\varepsilon_{xx}^2 + \varepsilon_{yy}^2 + \varepsilon_{zz}^2)/3]^{1/2}$ (in the principal axis orientation).

Two-dimensional powder diffraction patterns were integrated along 2θ using the *XMAS* software. Le Bail fits were performed using the *FullProf* software package (Rodríguez-Carvajal, 1993). A three-phase model was used for the refinement of *terra sigillata* slip (hematite, corundum and quartz) and body (hematite, anorthite and quartz), with the peak shape modelled with a pseudo-Voigt function. In the case of flint data refinement, the peak shape was modelled with a simple isotropic size model in order to extract the apparent size of the coherently diffracting domains.

4. Results and discussion

4.1. *Terra sigillata* pottery

The complementarities between monochromatic and Laue micro-diffraction techniques to study the crystalline composition of *sigillata* ceramics are illustrated in Fig. 2. Well defined powder diffraction rings can be obtained in monochromatic mode from the slip of *sigillata* ceramics, while almost no diffraction signal is recorded in Laue mode (Figs. 2a and 2b). Only rare sub-micrometre quartz crystals can be spotted. This confirms that the slip of *sigillata* ceramics is mainly composed of nanocrystalline phases (hematite, corundum), dispersed in a

glassy matrix (Sciau, Relaix *et al.*, 2006). On the other hand, the information obtained in monochromatic mode with a microbeam from the body of the ceramic is quite complex (Fig. 2c). Highly spotty diffraction rings are observed, indicating the presence of larger crystals (>1 µm), together with nanocrystalline phases. In this case, a Laue pattern may provide better quantitative crystallographic information (Fig. 2d).

In order to get new insights into the role of hematite in producing the colour of *terra sigillata* ceramics, an X-ray fluorescence map on a slip/body cross section sample was measured. As shown in Fig. 3(a), the Fe concentration is significantly higher in the slip than in the body. Then, the distribution of hematite crystals was followed using monochromatic and Laue micro-diffraction techniques (Figs. 3b and
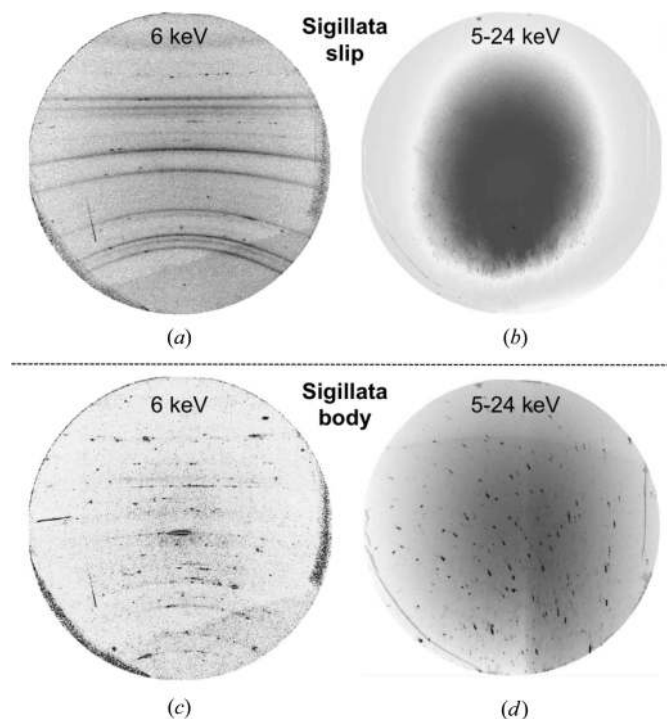
Table 1
Experimental details and scanning conditions for the different samples investigated.

	Iron nail	Flint	Pre-*sigillata* Bram	Pre-*sigillata* La Graufesenque	*Sigillata*
Detector position (°)	60	70	70	70	70
Sample position (°)	15	30	30	30	30
Sample–detector distance (mm)	80	80	80	80	80
Laue energy range (keV)	5–24	5–24	5–24	5–24	5–24
X–Y scan (Laue) (µm)	5 × 5	2 × 2	2 × 3	2 × 3	2 × 2
Recording time (for 1 pattern) (s)	1	1	0.1	0.5	1
Monochromatic energy (keV)	6	6	–	–	6
X–Y scan (mono) (µm)	5 × 5	5 × 5	–	–	3 × 5
Recording time (s)	60	100	–	–	90

(a) (b) (c) (d)

Figure 2
Diffraction patterns from *terra sigillata* slip and body, obtained by using Laue single-crystal micro-diffraction and monochromatic powder micro-diffraction. In monochromatic mode, homogeneous diffraction rings of hematite are clearly visible for the *sigillata* slip. The Laue pattern has been collected from a quartz crystal in the body.

Table 2
Cell parameters of the hematite phase from a high-quality *sigillata* ceramic.

A Le Bail fit was carried out for all the patterns extracted from the powder diffraction maps performed on the slip and on the body. The *a/c* value extracted after unit-cell shape refinement from Laue data is also given. The dispersion is shown with the maximum and minimum values given in brackets.

Data type		Slip	Body	Reference† 0 mol% Al	Reference† 5 mol% Al	Reference† 9 mol% Al
Monochromatic	No. patterns	25	25	–	–	–
	a (Å)	5.0303 (5.0295–5.0310)	5.0408 (5.0377–5.0428)	5.0395	5.0305	5.0251
	c (Å)	13.6916 (13.6809–13.6974)	13.7261 (13.6983–13.7436)	13.7544	13.7197	13.6926
	a/c	0.3674 (0.3672–0.3677)	0.3672 (0.3666–0.3680)	–	–	–
Laue	No. patterns	–	109	–	–	–
	a/c	–	0.3654 (0.3616–0.3684)	–	–	–

† *a* parameter: Schwertmann (1979); *c* parameter: Sciau, Relaix *et al.* (2006).

3*c*). The intensity of the 104 reflection extracted from powder diffraction data is plotted in Fig. 3(*b*). In agreement with the X-ray-fluorescence Fe mapping (Fig. 3*a*), Fig. 3(*b*) shows that the amount of nanocrystalline hematite is higher in the slip than in the body. The distribution at the micrometre scale of nanocrystalline hematite in the slip is also more homogeneous than in the body. The mapping of the same region of interest using Laue micro-diffraction shows a few larger hematite crystals (~1–3 µm size), randomly oriented, mainly in the ceramic body (Fig. 3*c*).

The cell parameters of hematite were refined from both monochromatic data (Le Bail fit) and Laue data (unit-cell shape refinement). The refinement results are shown in Table 2. The cell parameter values extracted from the slip do

not show any strong dispersion (Table 2), which means that the hematite composition is quite homogeneous at the micrometre scale all over the slip. However, the average values of the *a* and *c* parameters of nanocrystalline hematite are slightly lower than the reference one. The presence of Al and Ti atoms in substitution for Fe in the structure of hematite in *terra sigillata* ceramics has been previously reported (Sciau, Relaix *et al.*, 2006; Zoppi *et al.*, 2006). The presence of aluminium in the hematite structure is known to be responsible for a decrease of the unit-cell parameters (Schwertmann, 1979). Using the relationship between the amount of substituted aluminium and the *a* parameter of hematite proposed by Schwertmann (1979), we calculated that nanocrystalline hematite in *terra sigillata* slips is replaced on average with about 5 mol% of Al. This is slightly lower than the values obtained by electron energy loss spectroscopy (EELS) (~8%) at the nanometre scale (Sciau, Relaix *et al.*, 2006). This may be related to the additional presence of Ti atoms through substitution, which may counter-balance the role of Al and its effect on the *a* parameter evolution. The *c* parameter of hematite is less affected by the presence of substituted atoms (Schwertmann, 1979), in particular Ti atoms (Sciau, Relaix *et al.*, 2006). By using the evolution of the *c* parameter as a function of the amount of Al proposed by Sciau, Relaix *et al.* (2006), the amount of substituted Al at the micrometre scale in *terra sigillata* slip is estimated to be 8–10 mol%, in better agreement with EELS results.

The cell parameters of nanocrystalline hematite from the ceramic body show much less deviation compared to the reference structure (Table 2). This is in agreement with a lower Al-to-Fe substitution (Leon, 2010; Leon *et al.*, 2015). However, the cell parameters values are more dispersed than the ones extracted from the slip. In addition, the *a/c* parameter ratio extracted from larger hematite crystals present in the body (Laue data) shows a much larger dispersion than that from the nanocrystalline part (Table 2). This is in agreement with the fact that the body is obtained from a coarser clay preparation. These results also suggest that sub-micrometre size hematite in the body may originate from the transformation during firing of iron oxides already present in the raw clay, more intrinsically heterogeneous but less sensitive to any further substitution of Al.
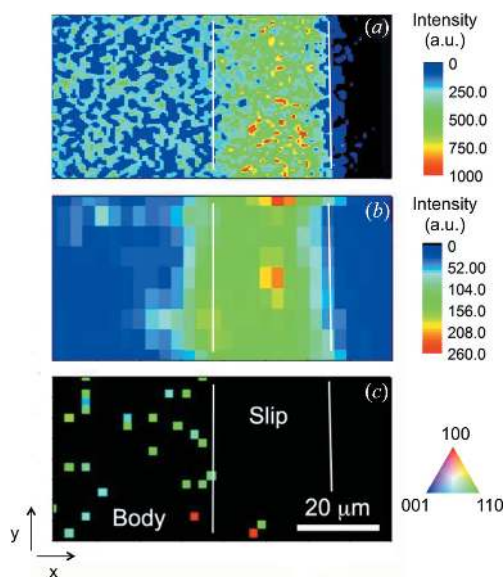

Figure 3
Distribution of iron and hematite Fe₂O₃ in the slip and the body of a high-quality *terra sigillata* ceramic, based on (*a*) X-ray fluorescence (recorded using the white beam), (*b*) monochromatic micro-diffraction (intensity of the 104 reflection) and (*c*) Laue micro-diffraction (the black zone is related to the absence of single-crystal signal). The X-ray fluorescence map clearly shows the difference between the slip and the body. Hematite is mainly in a nanocrystalline form in the slip, but also forms larger crystals in the body.

By comparing the results obtained for the slip (fine decanted clay) and the body (coarser clay), we note an evolution of the heterogeneity in composition of hematite (given by the cell parameter dispersion) as a function of the grain size: the larger the hematite crystals, the higher the heterogeneity. This is the first time such Laue information has been analysed together with monochromatic powder diffraction, which has been extensively used in recent work (Leon *et al.*, 2015).

We have shown that the distribution and composition at the micrometre scale of hematite in a nanocrystalline form is quite homogeneous all over the slip. The presence of Al atoms substituting for Fe in the structure results in a shift of the colour toward smaller wavelength (Barron, 1984). We conclude that the deep-red tone of *terra sigillata* slips is a direct result of the presence of homogeneously dispersed nanocrystals of Al-substituted hematite in a glassy matrix. On the other hand, the smaller amount of nanocrystalline hematite in the ceramic body, more heterogeneous in composition and without significant Al substitution, accounts for its lighter shade of red (Fig. 1). A shift towards purple wavelengths is observed with increasing particle size and agglomeration (Morris *et al.*, 1985). As no darkening is observed, the presence of larger crystals in the body, as spotted by Laue micro-diffraction, does not seem to contribute to the final colour.

Contrary to iron oxides that formed during the firing process, other phases, like quartz, are already present in the raw material. Under the heating and cooling stages, the amount and the size distribution of some of these original phases is not affected, which provides a unique way to get insight into the clay processing before firing. The distribution and orientation of quartz crystals in two pre-*sigillata* cross sections (Bram and La Graufesenque workshops) and one high-quality *sigillata* (La Graufesenque) were investigated using Laue micro-diffraction. As shown in Fig. 4, quartz is mainly present as large crystals (a few micrometres in size) concentrated in the ceramic body. The absence of large quartz crystals in the slips of the two pre-*sigillata* and of the *sigillata* ceramics confirms that they were obtained from a fine-decanted part of the raw clay from which large crystals were eliminated. On the other hand, we can see that quartz crystals

are found in much larger quantities in the bodies of the two pre-*sigillata* samples than in the body of the high-quality *sigillata* ceramic. This is a clear indication of a change in the clay preparation in order to produce high-quality *sigillata*, with the extraction of a finer fraction of the clay for the body. Comparing the two pre-*sigillata* samples, a smaller amount of quartz seems to be present in the Bram ceramic body, the black region being related to the absence of quartz diffracting signal. This may be due to the presence of quite large quantities of a calcite phase in Bram pottery bodies (Leon, 2010). Stress analysis carried out on quartz crystals (not shown here) did not provide any pertinent information correlating the annealing temperature, which may relax preexisting stresses, with the presence of hard quartz crystals embedded in a soft matrix.

4.2. Flints

Although the Si element, the main chemical component of flints, cannot be detected by X-ray fluorescence with the current setup, fluorescence scans were performed on several regions of the archaeological and geological flints in order to check for any inhomogeneity coming from impurities. The distributions of Ca and Ti were found to be quite uniform across the samples (not shown). A few zones with higher concentration of Fe were detected, indicating the presence of hematite. Except for these few Fe-rich zones, both archaeological and geological flints are quite homogeneous in composition at the micrometre scale.

Heated and non-heated archaeological flints (Fig. 1*b*) were first investigated by monochromatic powder X-ray micro-diffraction. A powder diffraction pattern could be obtained at each point of the investigated areas for both non-heated and heated samples, which means that nanocrystalline quartz is present throughout the samples. A typical diffraction pattern of quartz obtained from nanocrystalline material (monochromatic powder diffraction mode) is shown in Fig. 5(*a*). A Le Bail fit was performed and the cell volume as well as the apparent size of the coherently diffracting domains (CDD) were extracted (not shown). No significant change in relation with the heating process was noticed between the non-heated and the heated archaeological samples. The same zones were scanned using Laue single-crystal micro-diffraction, and the corresponding diffraction pattern from a large crystal is shown in Fig. 5(*a*). The distribution and orientation extracted from Laue data of larger detritic quartz crystals obtained from both non-heated and heated archaeological flints are shown in Fig. 5(*b*). Black zones are related to the exclusive presence of nanocrystalline quartz (no significant Laue diffraction signal can be detected). Some of the large crystals are isolated, while others seem to form clusters. Their size varies strongly, from a few micrometres (*e.g.* Fig. 5*b*, non-heated flint, NH) to tens of micrometres (*e.g.* Fig. 5*b*, heated flint, H), without showing any preferred orientation. The equivalent lattice strain extracted from Laue data is shown in Fig. 5(*c*). Larger values are found in the case of the non-heated sample. Moganite, only present as a minority phase in this type of flint (Schmidt,
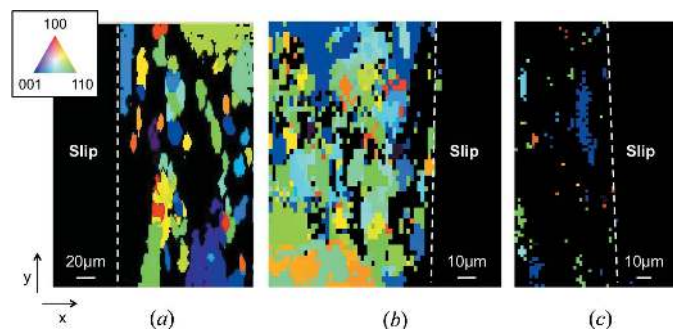

Figure 4
Quartz single-crystal distribution in the body of (*a*) a pre-*sigillata* from Bram, (*b*) a pre-*sigillata* from La Graufesenque and (*c*) a high-quality *sigillata* from La Graufesenque, obtained from Laue micro-diffraction data. The dashed line shows the boundary between slip and body.

Lea *et al.*, 2013), was not detected using either Laue or monochromatic micro-diffraction.

In order to better understand the role of the heating process, geological flints were also investigated, first using X-ray powder micro-diffraction mapping. All powder patterns were processed through a Le Bail fit in order to check for any structural effect on the nanocrystalline quartz phase due to the heating process. The evolution of the cell volume and the apparent domain size in the investigated areas for the heated (673 K) and non-heated samples is shown in Fig. 6. The cell volume is quite homogeneous and does not show significant variation, ranging from 110.8 to 111.2 $\mathring{A}^3$ and from 110.8 to 110.9 $\mathring{A}^3$ for the non-heated (Fig. 6*a*) and the heated samples (Fig. 6*b*), respectively. We conclude that the cell volume of nanocrystalline quartz is not affected by the heating process, which is in agreement with a previous *in situ* powder diffrac-

tion study for which a large beam was used (Roqué *et al.*, 2011). On the other hand, we find a global increase in the apparent size of the CDD after the heating process (Fig. 6*c*). Although we cannot exclude possible variation of the particle size between different samples, this result suggests that the heating process affects the nanocrystalline part of the flint, with the emergence of larger CDD. This effect was not observed during *in situ* experiments performed at Diamond Light Source on a fragment of the same geological sample heated at similar temperature (Roqué *et al.*, 2011). These experiments were carried out using a macro beam, and as the diffracted volume contains many large detritic crystals, their contribution to the diffraction pattern is predominant. The diffraction peak broadening due to the presence of nano-crystals affects only the diffraction peak tails, and a small
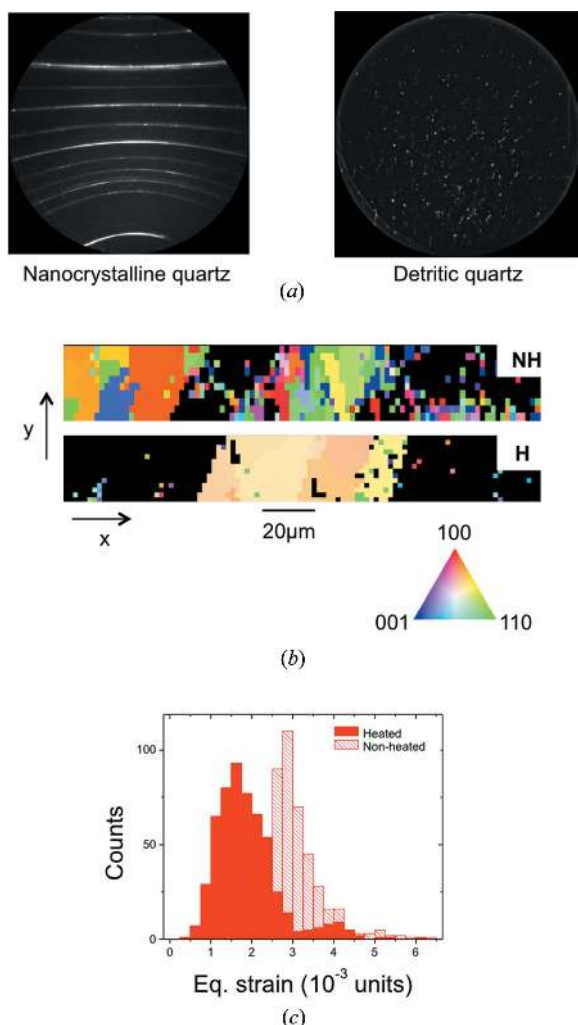

Figure 5
(*a*) Diffraction patterns obtained in monochromatic mode (nanocrystalline quartz) and in Laue mode (large detritic quartz crystals). (*b*) Distribution and orientation of quartz crystals in non-heated (NH) and heated (H) archaeological flints, extracted from Laue micro-diffraction data. Black zones correspond to the exclusive presence of nanocrystalline quartz. (*c*) The histogram of the equivalent lattice strain extracted from Laue data indicates some additional strain for large quartz crystals in the non-heated flint.
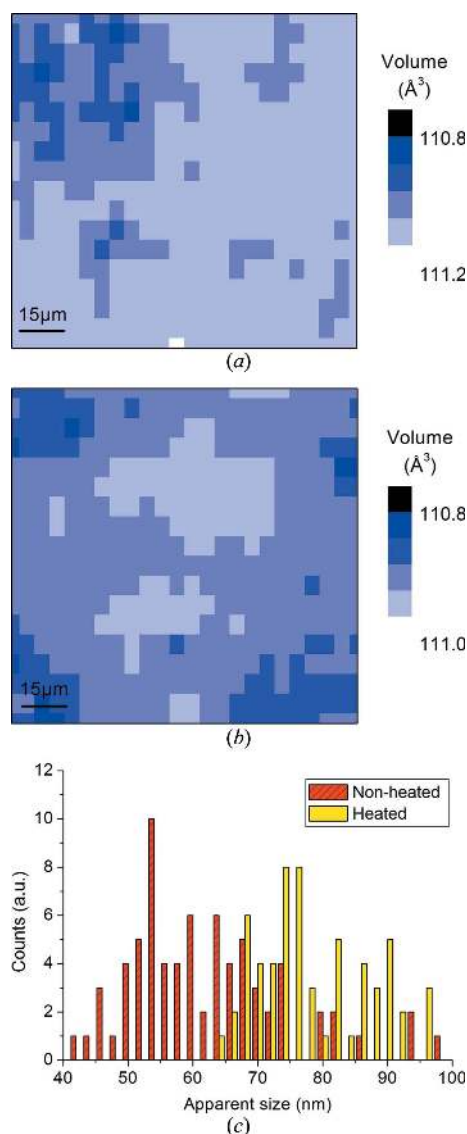

Figure 6
Evolution of the cell volume of quartz extracted from monochromatic data in (*a*) a non-heated and (*b*) a heated geological flint. The cell volume is not affected by the heating process. (*c*) Histogram of the apparent size of the coherently diffracting domains obtained after refinement of the powder data, showing a slight increase after the heating process.

variation of the size of these crystals is then very difficult to observe. In the present study, thanks to the small beam size, only the nanocrystalline phase contributes to the powder diffraction patterns, and even if the size of the CDD increases only slightly, the effect is measurable.

This larger-size domain effect has not been detected for heated archaeological flints. We interpret this as an effect of the lower temperature treatment applied to archaeological flints (~523 K instead of 673 K for the geological sample). Schmidt, Slodczyk *et al.* (2013) have shown by thermogravimetry that in the 473–523 K temperature range only a small fraction of silanol Si—OH is released, mainly at the grain interfaces. Consequently, only a few Si—O—Si bonds can be created, resulting in a 'closing of the porosity' without significantly affecting the apparent size of the CDD. At 673 K, a much larger amount of silanol is lost, not only at the grains' surface but also from inside the grains. Our XRD results suggest that at such temperature the larger number of Si—O—Si bonds created leads to long-range order and contributes to the expansion of the CDD. Additional experiments at intermediate temperatures will be necessary to support this result.

The orientation maps of detric quartz crystals extracted from Laue data for the geological samples are shown in Fig. 7. The corresponding strain orientation distributions for the three main axis components are also reported. While the strain distribution does not show any strong correlation with crystal orientations, significant variations of the equivalent lattice strain between the non-heated and the heated samples

are found (Fig. 7). An additional maximum at higher strain values can be seen on the equivalent strain histogram of the non-heated sample, which is not observed for the heated one. Similar results have been found for the archaeological flints (Fig. 5c). The most peculiar characteristics of rock are its initial stress condition. Indeed, a rock is always under a natural state of stress (residual stress), primarily resulting from the gravitational and tectonic forces to which it is subjected. Previous micro-Laue studies evidencing residual elastic strain and stress in deformed natural quartz have been carried out (Kunz, Chen *et al.*, 2009; Chen *et al.*, 2012). We conclude that the residual strain present in the detric quartz crystals is partially released as a consequence of the heating process. Contrary to what we observed for the nanocrystalline quartz phase, the large detric quartz crystals behave similarly in archaeological and geological flints, irrespective of the final heating temperature reached.

Combining monochromatic and Laue micro-diffraction techniques has allowed us to detect structure modifications of flints occurring at both the nano- and the micrometre scale. Such an approach provides new insights into how the flint's mechanical properties change as a consequence of the heating process. By de-correlating the diffracted signal coming from nanocrystalline quartz and larger detric quartz, we found evidence for a domain size increase for nano quartz in the case of geological flint heated at higher temperature, and a relaxing of the residual strain in the larger detric quartz for both archaeological and geological flints. This is also a way to get a
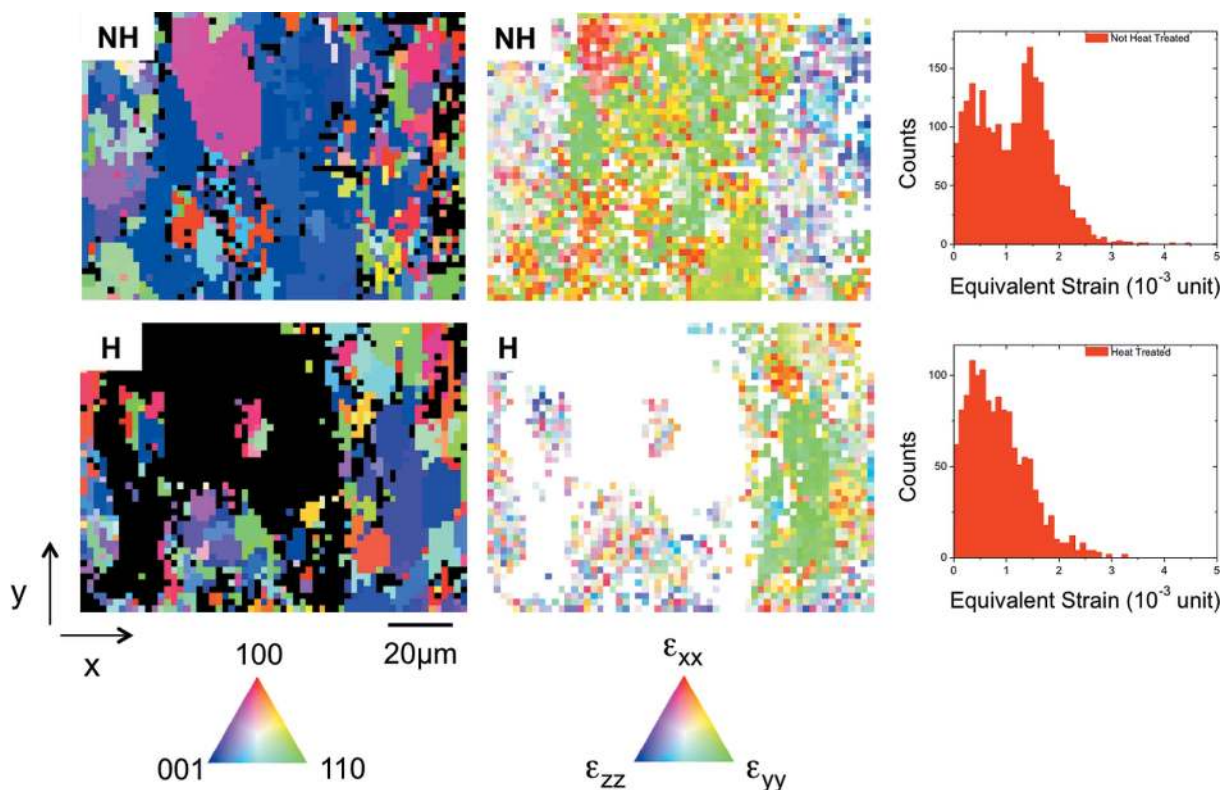

Figure 7
Distribution and orientation of quartz crystals in non-heated and heated geological flints, obtained from Laue micro-diffraction data. The corresponding strain distribution (principal axis) and equivalent strain histogram are also shown. Black zones in the orientation map and white zones in the equivalent strain map are related to the absence of quartz single crystals.
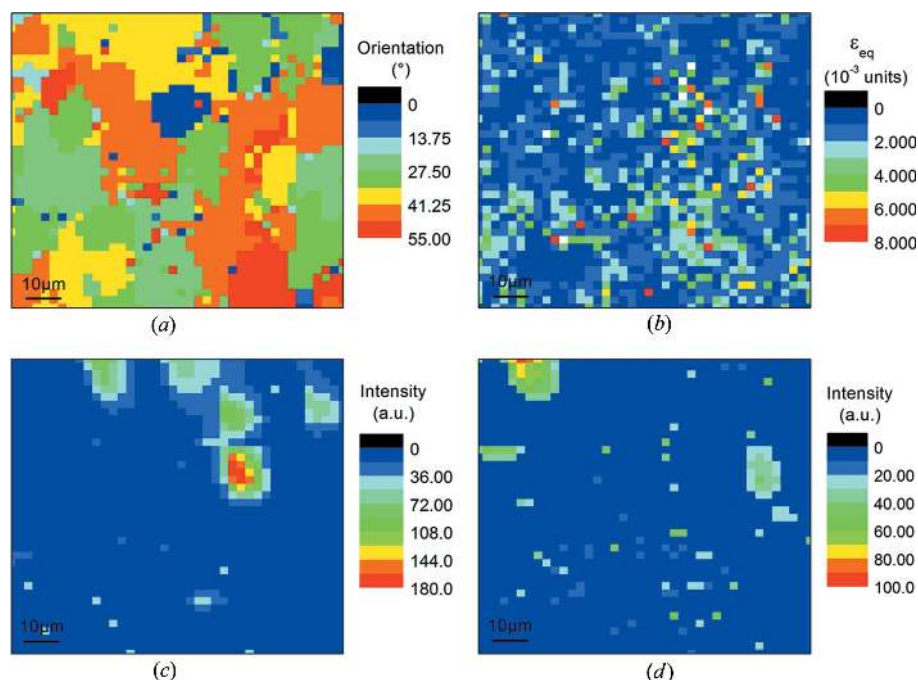
Figure 8
(*a*) Ferrite crystal distribution at the surface of a Roman nail, obtained by plotting the out-of-plane crystal orientation (angle of the [100] crystallographic direction with the sample surface normal) from Laue micro-diffraction data. (*b*) Corresponding equivalent strain calculated from Laue data. (*c*) Intensity map of the 022 reflection of the cementite phase (monochromatic mode). (*d*) Intensity map of the 202 reflection of the cementite phase (monochromatic mode). Cementite is highly textured.

cementite in a nanocrystalline form). The absence of additional phases besides ferrite and cementite in the analysed zones is characteristic of a slow cooling step during the fabrication process (Douin *et al.*, 2010). As shown in Fig. 8(*a*) where the orientation angle of the crystals has been plotted, ferrite crystals are quite disoriented from each other, with an angle ranging from 0 to 55°. The presence of nanocrystalline perlite regions distributed among the disoriented single-crystal-like ferrite domains is in agreement with a surface carburation process carried out by repetitive hammering and reheating.

As shown in the distribution maps obtained from the 022 (Fig. 8*c*) and the 202 (Fig. 8*d*) reflections, cementite is highly textured. It has been shown that the orientation of cementite crystals can be related to the orientation of neighbouring ferrite grains (Douin *et al.*, 2010). We then attributed the strong texture of the cementite phase to the presence of adjacent ferrite crystals. Nevertheless, without knowing the relative position in three dimensions of the cementite and ferrite domains, the exact orientation relationship could not be devised.
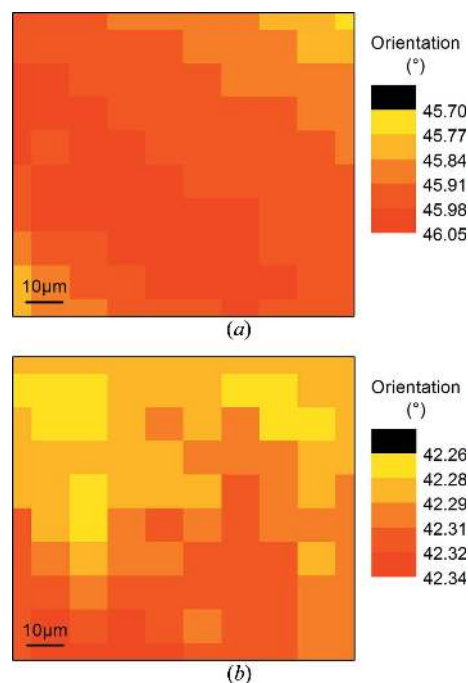
better understanding of the practical knowledge of Neolithic societies from the northwestern Mediterranean zone. Indeed, rather slow and controlled heating and cooling stages have to be applied in order to proceed to the closing of the porosity and get the appropriate hardening and cutting properties. Keeping a homogeneous temperature between the surface and the heart of the material in the 473–523 K range will limit the quantity of water molecules trapped inside and ensure no breaking of the flint during the heating process (Schmidt, Slodczyk *et al.*, 2013). The absence of an increase of the CDD in the nanocrystalline quartz phase and the release of the strain in large quartz crystals after the heating phase is clear evidence of a slow and controlled fabrication process.

4.3. Roman nail

We investigated six different regions of the polished surface of a Roman nail using Laue and monochromatic micro-diffraction (Fig. 1*c*, left). Similar results were obtained for all the six investigated zones, so only one of them is presented here. All Laue patterns were indexed with the ferrite structure (*α*-Fe), present as large single crystals. In addition, both ferrite and cementite (Fe₃C) in a nanocrystalline form were identified by monochromatic powder diffraction. No other phase could be found. The resulting maps are shown in Fig. 8. We observe that the polished nail surface is composed of ferrite crystals (10–20 µm size; Fig. 8*a*) and nanocrystalline cementite-rich zones (the larger ones around 10–20 µm size; Figs. 8*c* and 8*d*), which is characteristic of pearlite colonies (a mix of ferrite/

Figure 9
Out-of-plane crystal orientation distribution of ferrite obtained from Laue micro-diffraction data from two different zones of the nail core. Only very large ferrite grains are found, showing non-significant variations in orientation.

The equivalent strain of larger ferrite crystals was calculated from the Laue data. The corresponding map is plotted in Fig. 8(b). Strain is not homogeneously spread, and some crystals appear to be less strained than others. The presence of pearlites is known to strengthen the steel by preventing the propagation of dislocations in ferritic crystals, the hardness of cementite being higher. Beside the intrinsic non-homogeneity of the material, we conclude that the non-homogeneous strain dispersion in ferrite crystals may be related to the presence or the absence of adjacent pearlite domains. Again, three-dimensional information is required to clarify this point.

Investigation of the bulk of the Roman nail (Fig. 1c, right) showed quite different results. Only very large grains of ferrite (~100 µm size) could be identified using Laue single-crystal micro-diffraction. The variation in orientation of ferrite crystals identified in two different zones is shown in Figs. 9(a) and 9(b). In both cases, the angle orientation is changed by less than 0.4°, in accordance with the presence of a unique quite large single crystal. If we combine this result with the complete absence of cementite, we can conclude that the ductility of the bulk is higher than that of the surface, with no limits for possible dislocations to propagate over large area.

Through the combined measurement carried out using both monochromatic and Laue micro-diffraction at the surface and inside the bulk of the material, a better understanding of the carburation process is obtained over a representative area of the sample. We have shown that the carburation is mainly a surface process, leading to dispersed 10–20 µm-size domains of single-crystal ferrite and nanocrystalline cementite. This study underlines the metallurgical properties of a nail obtained using surface treatment during Roman times: an external hard surface due to the presence of pearlite domains covering a ductile core made only of large micrometric ferrite grains.

5. Conclusion

We have shown that combining monochromatic diffraction, Laue diffraction and the use of an X-ray micro-beam on the same instrument offers new possibilities to investigate the crystalline phases of heterogeneous cultural heritage artefacts on a micrometre scale. This hybrid methodology allows us to probe the existence, or absence, of micrometric and/or nanometric phases and to interpret the associated crystallographic structures in the sample probed volume. Conventional diffraction based on a sub-millimetre X-ray beam size is not able to provide such information because of overlap in the measured signal. Three different types of ancient materials have been investigated in the present study. The description of their organization at the micrometre scale provides new information in relation to the mechanical properties of the material and the function of the artefact: the colour of *terra sigillata* ceramics, the hardening of Neolithic flints and the strength of Roman nails. Although already common in scientific domains such as applied materials science and mineralogy (Tamura *et al.*, 2003; Kunz, Chen *et al.*, 2009), we are convinced that Laue micro-diffraction, if combined with powder monochromatic mode, has a huge potential in the field of cultural heritage materials. Moreover, high spatial resolution mapping using micro-diffraction with poly- and monochromatic synchrotron X-rays beam can usefully complete the panel of strain measurement techniques already in use in the discipline of rock mechanics (Zang & Stephansson, 2010). However, although the two-dimensional description of the microstructure of the material is established, the depth information is still missing. This could be achieved by implementing three-dimensional methods developed on non-rotating samples (Larson *et al.*, 2002). A more quantitative analysis of the structure, from both monochromatic and Laue data (Dejoie *et al.*, 2013), could also provide additional details on these heterogeneous and complex materials.

References

Baraldi, P. & Tinti, A. (2008). *J. Raman Spectrosc.* **39**, 963–965.
Barron, V. (1984). *Clays Clay Miner.* **32**, 157–158.
Bertrand, L., Cotte, M., Stampanoni, M., Thoury, M., Marone, F. & Schoder, S. (2012). *Phys. Rep. Rev. Sec. Phys. Lett.* **519**, 51–96.
Chen, K., Dejoie, C. & Wenk, H.-R. (2012). *J. Appl. Cryst.* **45**, 982–989.
Déchelette, J. (1903). *Rev. Etud. Anc.* **5**, 1–42.
Dejoie, C., Martinetto, P., Tamura, N., Kunz, M., Porcher, F., Bordat, P., Brown, R., Dooryhée, E., Anne, M. & McCusker, L. B. (2014). *J. Phys. Chem. C*, **118**, 28032–28042.
Dejoie, C., McCusker, L. B., Baerlocher, C., Kunz, M. & Tamura, N. (2013). *J. Appl. Cryst.* **46**, 1805–1816.
Dejoie, C., Sciau, P., Li, W. D., Noé, L., Mehta, A., Chen, K., Luo, H. J., Kunz, M., Tamura, N. & Liu, Z. (2014). *Sci. Rep.* **4**, 4941.
De Nolf, W. & Janssens, K. (2010). *Surf. Interface Anal.* **42**, 411–418.
Dooryhée, E., Anne, M., Bardiès, I., Hodeau, J. L., Martinetto, P., Rondot, S., Salomon, J., Vaughan, G. M. & Walter, P. (2005). *Appl. Phys. A*, **81**, 663–667.
Douin, J., Henry, O., Dabosi, F. & Sciau, P. (2010). *Eur. Phys. J. Appl. Phys.* **51**, 10902.
Gibaja, J. F. & Terradas, X. (2012). *C. R. Palevol.* **11**, 463–472.
Gilliver, K. (2002). *Caesar's Gallic Wars 58–50 BC.* London: Osprey Publishing.
Goudeau, P., Villain, P., Tamura, N. & Padmore, H. A. (2003). *Appl. Phys. Lett.* **83**, 51–52.
Hermet, F. (1934). *La Graufesenque, Condatomogos, Vases Sigillés, Graffites.* Paris: Librairie Ernest Laroux.
Ice, G. E., Budai, J. D. & Pang, J. W. L. (2011). *Science*, **334**, 1234–1239.
Ice, G. E. & Pang, J. W. L. (2009). *Mater. Charact.* **60**, 1191–1201.
Ingham, J. P. (2011). *Q. J. Eng. Geol. Hydrogeol.* **44**, 457–467.
Korsunsky, A. M., Hofmann, F., Song, X., Eve, S. & Collins, S. P. (2010). *J. Nanosci. Nanotechnol.* **10**, 5935–5950.
Kunz, M., Chen, K., Tamura, N. & Wenk, H. R. (2009). *Am. Mineral.* **94**, 1059–1062.

Kunz, M., Tamura, N. *et al.* (2009). *Rev. Sci. Instrum.* **80**, 035108.

Larson, B. C., Yang, W., Ice, G. E., Budai, J. D. & Tischler, J. Z. (2002). *Nature*, **415**, 887–890.

Lea, V. (2005). *Antiquity*, **79**, 51–65.

Leon, Y. (2010). PhD thesis, Université de Toulouse, France.

Leon, Y., Sciau, P., Goudeau, P., Tamura, N., Webb, S. & Mehta, A. (2010). *Appl. Phys. A*, **99**, 419–425.

Leon, Y., Sciau, P., Passelac, M., Sanchez, C., Sablayrolles, R., Goudeau, P. & Tamura, N. (2015). *J. Anal. At. Spectrom.* **30**, 658–665.

Liu, Z., Mehta, A., Tamura, N., Pickard, D., Rong, B., Zhou, T. & Pianetta, P. (2007). *J. Archaeol. Sci.* **34**, 1878–1883.

Lynch, P. A., Tamura, N., Lau, D., Madsen, I., Liang, D., Strohschnieder, M. & Stevenson, A. W. (2007). *J. Appl. Cryst.* **40**, 1089–1096.

MacDowell, A. A., Celestre, R. S., Tamura, N., Spolenak, R., Valek, B., Brown, W. L., Bravman, J. C., Padmore, H. A., Batterman, B. W. & Patel, J. R. (2001). *Nucl. Instrum. Methods Phys. Res. Sect. A*, **467–468**, 936–943.

Mirguet, C., Dejoie, C., Roucau, C., de Parseval, P., Teat, S. J. & Sciau, P. (2009). *Archaeometry*, **51**, 748–762.

Morris, R. V., Lauer, H. V., Lawson, C. A., Gibson, E. K., Nace, G. A. & Stewart, C. (1985). *J. Geophys. Res.* **90**, 3126–3144.

Pagès, G., Dillmann, P., Fluzin, P. & Long, L. (2011). *J. Archaeol. Sci.* **38**, 1234–1252.

Passelac, M. (1992). *Rei Cretariae Romanae Favtorvm Acta*, **31–32**, 207–229.

Passelac, M. (2004). *Peuples et Territoires en Gaule Méditerranéenne. Hommage à Guy Barruol*, supplément au numéro 35, edited by R. A. D. Narbonnaise, pp. 95–107. Montpellier: Université Paul-Valéry.

Passelac, M. (2007). *Les Imitations de Vaixella Fina Importada a la Hispania Citerior*, edited by M. Roca Roumens & J. Principal, pp. 17–45. Tarragona: Institut Català d'Arqueologia Clàssica.

Renoux, G. (2006). PhD thesis, Université Toulouse Le Mirail, Toulouse, France.

Renoux, G., Dabosi, F. & Pailler, J. M. (2004). *Rev. Archéo.* **28**, 141.

Ríos, S., Salje, E. K. H. & Redfern, S. A. T. (2001). *Eur. Phys. J. B*, **20**, 75–83.

Robach, O., Micha, J.-S., Ulrich, O. & Gergaud, P. (2011). *J. Appl. Cryst.* **44**, 688–696.

Rodríguez-Carvajal, J. (1993). *Physica B*, **192**, 55–69.

Roqué, J., Torchy, L., Roucau, C., Lea, V., Colomban, P., Regert, M., Binder, D., Pelegrin, J. & Sciau, P. (2011). *MRS Online Proceedings Library*, **1319**, mrsf10-1319-ww1309-1302.

Schaad, D. (2007). *La Graufesenque (Millau, Aveyron)*, Vol. I, *Condatomagos une Agglomération de Confluent en Territoire Rutène*. Pessac: Editions de la Fédération Aquitania.

Schmidt, P., Lea, V., Sciau, P. & Frohlich, F. (2013). *Archaeometry*, **55**, 794–805.

Schmidt, P., Slodczyk, A., Léa, V., Davidson, A., Puaud, S. & Sciau, P. (2013). *Phys. Chem. Miner.* **40**, 331–340.

Schwertmann, U. (1979). *Clays Clay Miner.* **27**, 105–112.

Sciau, P., Goudeau, P., Tamura, N. & Dooryhee, E. (2006). *Appl. Phys. A*, **83**, 219–224.

Sciau, P., Relaix, S., Roucau, C., Kihn, Y. & Chabanne, D. (2006). *J. Am. Ceram. Soc.* **89**, 1053–1058.

Tamura, N. (2014). *Strain and Dislocation Gradients from Diffraction Spatially Resolved Local Structure and Defects*, edited by R. Barabash & G. E. Ice, pp. 125–155. London: Imperial College Press.

Tamura, N., Celestre, R. S., MacDowell, A. A., Padmore, H. A., Spolenak, R., Valek, B. C., Meier Chang, N., Manceau, A. & Patel, J. R. (2002). *Rev. Sci. Instrum.* **73**, 1369–1372.

Tamura, N., Kunz, M., Chen, K., Celestre, R. S., MacDowell, A. A. & Warwick, T. (2009). *Mater. Sci. Eng. A*, **524**, 28–32.

Tamura, N., MacDowell, A. A., Spolenak, R., Valek, B. C., Bravman, J. C., Brown, W. L., Celestre, R. S., Padmore, H. A., Batterman, B. W. & Patel, J. R. (2003). *J. Synchrotron Rad.* **10**, 137–143.

Torrent, J. & Barrón, V. (2003). *Clays Clay Miner.* **51**, 309–317.

Vaxelaire, N., Gergaud, P. & Vaughan, G. B. M. (2014). *J. Appl. Cryst.* **47**, 495–504.

Walter, P., Martinetto, P., Tsoucaris, G., Brniaux, R., Lefebvre, M. A., Richard, G., Talabot, J. & Dooryhee, E. (1999). *Nature*, **397**, 483–484.

Welcomme, E., Walter, P., Bleuet, P., Hodeau, J. L., Dooryhee, E., Martinetto, P. & Menu, M. (2007). *Appl. Phys. A*, **89**, 825–832.

Xu, N., Cavallaro, G. P. & Gerson, A. R. (2012). *J. Mater. Res.* **27**, 2122–2130.

Zang, A. & Stephansson, O. (2010). *Stress Field of the Earth's Crust*. Dordrecht: Springer.

Zoppi, A., Lofrumento, C., Castellucci, E. M., Dejoie, C. & Sciau, P. (2006). *J. Raman Spectrosc.* **37**, 1131–1138.